


Communication

# Electrochemical Immunosensor Modified with Nitrogen-Doped Reduced Graphene Oxide@Carboxylated Multi-Walled Carbon Nanotubes/Chitosan@Gold Nanoparticles for CA125 Detection

Yingying Gu <sup>1,2,3,†</sup>, Guoao Gong <sup>1,3,†</sup>, Yuting Jiang <sup>1,3</sup>, Jianguang Qin <sup>1,3</sup>, Yong Mei <sup>1,3</sup> and Jun Han <sup>2,\*</sup> 

<sup>1</sup> School of Public Health, Medical College, Wuhan University of Science and Technology, Wuhan 430065, China; guyingying@wust.edu.cn (Y.G.); gongguoao@163.com (G.G.); jiangyutingjane@163.com (Y.J.); qinjianguang2021@163.com (J.Q.); meiyong2006@163.com (Y.M.)

<sup>2</sup> College of Resource and Environmental Engineering, Wuhan University of Science and Technology, Wuhan 430065, China

<sup>3</sup> Key Laboratory of Occupational Hazard Identification and Control of Hubei Province, Wuhan University of Science and Technology, Wuhan 430065, China

\* Correspondence: hanjun@wust.edu.cn

† These authors contributed equally to this work.

**Abstract:** Lung cancer is one of the malignant tumors with the highest mortality rate, and the detection of its tumor marker carcinoma antigen 125 (CA125) is significant. Here, an electrochemical immunoassay for CA125 was described. Nitrogen-doped reduced graphene oxide (N-rGO), carboxylated multi-walled carbon nanotubes (CMWCNTs) and gold nanoparticles (AuNPs) were applied to co-modify glassy carbon electrode (GCE), after incubation with Anti-CA125, the modified electrode was employed for the specific detection of CA125. The N-rGO@CMWCNTs (Nitrogen-doped reduced graphene oxide@carboxylated multi-walled carbon nanotubes) were used as a matrix, while CS@AuNPs (Chitosan@gold nanoparticles) with high conductivity and biocompatibility was immobilized on it through the reaction between carboxyl groups from CMWCNTs and amino groups, hydroxyl groups from chitosan (CS), resulting in the effect of double signal amplification. The immunosensor demonstrated excellent electrochemical performance with a linear detection range of 0.1 pg mL<sup>-1</sup>–100 ng mL<sup>-1</sup>, and the detection limit was as low as 0.04 pg mL<sup>-1</sup> (S/N = 3). It had been verified that this method had good precision and high accuracy, and the immunosensor could remain stable for 10 days. This research provided a new method for the detection of CA125 in serum.

**Keywords:** immunosensor; carcinoma antigen 125; nitrogen-doped reduced graphene oxide; carboxylated multi-walled carbon nanotubes; gold nanoparticles



**Citation:** Gu, Y.; Gong, G.; Jiang, Y.; Qin, J.; Mei, Y.; Han, J.

Electrochemical Immunosensor Modified with Nitrogen-Doped Reduced Graphene Oxide@Carboxylated Multi-Walled Carbon Nanotubes/Chitosan@Gold Nanoparticles for CA125 Detection. *Chemosensors* **2022**, *10*, 272. <https://doi.org/10.3390/chemosensors10070272>

Academic Editor: Danila Moscone

Received: 6 June 2022

Accepted: 7 July 2022

Published: 12 July 2022

**Publisher's Note:** MDPI stays neutral with regard to jurisdictional claims in published maps and institutional affiliations.



**Copyright:** © 2022 by the authors. Licensee MDPI, Basel, Switzerland. This article is an open access article distributed under the terms and conditions of the Creative Commons Attribution (CC BY) license (<https://creativecommons.org/licenses/by/4.0/>).

## 1. Introduction

Lung cancer is one of the tumors with the highest mortality rate [1,2], and the early diagnosis of it is significant for improving quality of life of the patients [3]. Most cases are not diagnosed until a late stage due to the lack of obvious symptoms in early-stage and effective physical examination [4]. As an important indicator for early diagnosis of cancer, tumor markers have received extensive attention in recent years [5,6]. CA125 was first discovered in 1983 as a cancer-specific biomarker [7], the high expression of which in serum predicts an increased risk of cancer. At present, the detection methods for CA125 mainly include enzyme-linked immunosorbent assay (ELISA) [8,9], electrochemiluminescence [10,11], radioimmunoassay [12,13] and electrochemical immunosensing technology [14,15], among which the electrochemical immunosensing technology is an important research direction for the majority of researchers due to its advantages such as low cost, short analysis time, high sensitivity, and miniaturization of instruments [16].

The working electrodes in electrochemical workstation usually need to be modified in order to improve their electrochemical performance and enhance conductivity of the

system. The substances modified on electrodes are mainly nanomaterials, among which carbon nanomaterials are the most widely used. Reduced graphene oxide (rGO) has the advantages of high specific surface area and good electrical conductivity [17]. However, the zero-band gap of rGO prevents its conductivity from being fully controlled. N-rGO can be obtained by introducing nitrogen atoms into rGO sheets. Due to the large difference between nitrogen atoms and carbon atoms in electronegativity, the doped nitrogen atoms in N-rGO can be used to replace carbon atoms to open the band gap and increase the charge density on adjacent carbon atoms [18]. Therefore, N-rGO has stable and excellent electrical conductivity, which is able to promote signal amplification for immunosensors. Multi-walled carbon nanotubes (MWCNTs) have the advantages of high electrical conductivity and great stability but poor solubility. CMWCNTs can be obtained by modifying carboxyl groups (-COOH) on MWCNTs, which can improve their biocompatibility and be used to fix biomolecules. The functionalized carboxyl groups of CMWCNTs can not only improve their solubility, but also react with specific molecules, such as hydroxyl groups and amine groups [19]. Moreover, CMWCNTs have a large surface area to volume ratio, which can promote electron transfer and improve the sensitivity of immunosensor. Furthermore, the CMWCNTs can be introduced into N-rGO and used as bridges for electron transport, which takes advantage of their structural features to obtain a high specific surface area and excellent electrical conductivity complex that cannot be obtained by a single component. The primary amine group of CS acts as a reducing agent and capping agent, which is able to reduce  $\text{Au}^{3+}$  in chloroauric acid trihydrate ( $\text{HAuCl}_4 \cdot 3\text{H}_2\text{O}$ ) to AuNPs [20]. Meanwhile, CS is rich in amino groups (-NH<sub>2</sub>) and hydroxyl groups (-OH), and they are able to react with the carboxyl groups (-COOH) from CMWCNTs. In addition, the positively charged amine groups of CS can electrostatically adsorb with negatively charged carbon nanomaterials in a weakly acidic environment [21], further improving the dispersibility of the system. As a result, N-rGO@CMWCNTs and CS@AuNPs can form a compact and stable composite film on the surface of GCE.

In this research, a novel electrochemical immunosensor modified with N-rGO@CMWCNTs/CS@AuNPs was fabricated, which can realize the ultrasensitive detection of CA125 in serum.

## 2. Materials and Methods

### 2.1. Reagents

CA125 and its capture antibody were purchased from Sangon Biotech Co., Ltd. (Shanghai, China). CYFRA21-1 was purchased from Key Bio Co., Ltd. (Beijing, China). Graphene oxide (GO) and carboxylated multi-walled carbon nanotubes (CMWCNTs) were purchased from Xianfeng Nanotechnology Co., Ltd. (Nanjing, China).  $\text{CH}_3\text{COOH}$ ,  $\text{HAuCl}_4 \cdot 3\text{H}_2\text{O}$ , Urea, Glucose (Glu), Ascorbic acid (AA), Uric acid (UA), N,N-Dimethylformamide (DMF), 1-(3-Dimethylaminopropyl)-3-ethylcarbodiimide hydrochloride (EDC) and N-hydroxysuccinimide (NHS) were purchased from Macklin Co., Ltd. (Shanghai, China). Chitosan (CS) and Bovine serum albumin (BSA) were purchased from Sigma-Aldrich Co., Ltd. (St. Louis, MO, USA). A 0.01 M Phosphate buffer solution (PBS, pH = 7.4) was purchased from Phygene Biotechnology Co., Ltd. (Fuzhou, China). The PBS containing 5 mM  $[\text{Fe}(\text{CN})_6]^{3-/4-}$  and 0.1 M KCl was selected as an electrolyte solution. The water used in the whole experiment was ultrapure water (18.25 M $\Omega$ .cm).

### 2.2. Instruments

The electrochemical technologies including cyclic voltammetry (CV), differential pulse voltammetry (DPV) and electrochemical dissolution/deposition were accomplished by CS150H electrochemical workstation from Corrtest Instrument Co., Ltd. (Wuhan, China). The three-electrode system consisted of a glassy carbon working electrode, a saturated Ag/AgCl reference electrode and a platinum wire counter electrode. The scanning electron microscope (SEM) images of the synthesized nanocomposites and the modified GCE were acquired by Gemini SEM 300 (Zeiss, Jena, Germany).

### 2.3. Synthesis of N-rGO@CMWCNTs

In addition, 20 mg GO and 20 mg CMWCNTs were added into 40 mL ultrapure water, and ultrasound above-mentioned solution for 1 h to obtain a uniform dispersed mixture. Next, 1 g urea was added into this mixture under vigorous stirring; continue stirring until they were well mixed. Then, the mixture was transferred into 180 °C autoclave for 12 h. After cooling to room temperature, centrifuge to get the precipitation (4000 rpm, 30 min), followed by rinsing with ultrapure water 3 times. The N-rGO@CMWCNTs was then obtained after vacuum drying at 50 °C for 24 h. Finally, 5 mg synthesized nanocomposite was dissolved into 1 mL DMF and treated with ultrasound for 30 min.

### 2.4. Synthesis of CS@AuNPs

CS@AuNPs were synthesized using procedures previously reported in the literature [22]. In brief, 50 mg CS was dissolved in 10 mL 1% (V/V) acetic acid, and stirred for 30 min to obtain a uniform dispersed mixture. Then, 200 µL 0.01 M H<sub>2</sub>AuCl<sub>4</sub>·3H<sub>2</sub>O was added into the mixture drop by drop; continue stirring for 24 h. The color of the solution gradually changed from pale yellow to pink, indicating the formation of AuNPs successfully.

### 2.5. Analytical Procedure

Before modification, the GCE was polished to mirror with 0.3 µm and 0.05 µm Al<sub>2</sub>O<sub>3</sub> wet powder successively, and ultrasonic rinsing was performed in 50% HNO<sub>3</sub>, 95% C<sub>2</sub>H<sub>5</sub>OH, and ultrapure water for 5 min each. Next, the electrochemical dissolution/deposition (2 V for 60 s, −0.9 V for 30 s) and CV (−0.9 V–1.1 V, 100 mV s<sup>−1</sup>) were carried out in 3% H<sub>2</sub>SO<sub>4</sub> sequentially. The combination of these two steps could achieve dual activation of the GCE, as well as shorten the time of electrode preparation compared to a single CV. The application of potentiostatic deposition led to the formation of a microporous structure on the electrode surface, which was able to increase effective surface area and improve adsorption performance of the GCE. Subsequently, 4 µL 5 mg mL<sup>−1</sup> N-rGO@CMWCNTs was dropped onto the surface of GCE, followed by drying at 50 °C for 30 min. Then, the electrode was immersed into PBS containing 0.03 M EDC and 0.03 M NHS for 3 h to activate carboxyl groups of the modified materials. After being cleaned with PBS, 5 µL CS@AuNPs was dropped onto the electrode surface, followed by drying at 50 °C for 15 min. Finally, 4 µL 50 µg mL<sup>−1</sup> Anti-CA125 was incubated on the modified electrode at 4 °C overnight. On the next day, 6 µL 1% (W/V) BSA solution was added to the modified electrode to block the non-specific binding sites. After 30 min, it was cleaned with PBS and dried at 37 °C.

On the other hand, 1 mg mL<sup>−1</sup> CA125 standard solution was gradiently diluted with PBS, and a series of CA125 solutions with different concentrations were then obtained (0.1 pg mL<sup>−1</sup>–100 ng mL<sup>−1</sup>). Subsequently, 4 µL of them were added to the modified electrode surface separately, followed by incubation at 37 °C for 30 min. After it, the electrochemical signals of the blank and each concentration were recorded by DPV in the electrolyte solution, which contained 5 mM [Fe(CN)<sub>6</sub>]<sup>3−/4−</sup> and 0.1 M KCl (0.05 V–0.45 V).

### 2.6. Collection of Serum Samples

The blood samples of normal people and 10 patients with lung cancer were obtained from Tianyou Hospital affiliated with Wuhan University of Science and Technology. To collect serum samples, the blood samples were centrifuged to remove some proteins (4000 rpm, 15 min). The clear supernatants were then collected, followed by storage at −20 °C. All the people had signed the informed consent.

## 3. Results and Discussion

### 3.1. Sensing Schemes

In this study, an ultrasensitive electrochemical immunosensing platform based on the modification of N-rGO@CMWCNTs/CS@AuNPs was put forward. Figure 1 outlined the construction process of this immunosensor. Sulfhydryl groups (−SH) of Anti-CA125 could

react with AuNPs to form Au-S bonds. Subsequently, when the corresponding CA125 was incubated on the electrode surface, immune complexes could be formed between them, which would hinder the electron transfer and reduce the measured current signal. The more CA125, the more immune complexes formed, the stronger blocking effect on electron transfer, and the lower DPV signal obtained. Based on this principle, the quantitative detection of CA125 in serum could be realized.

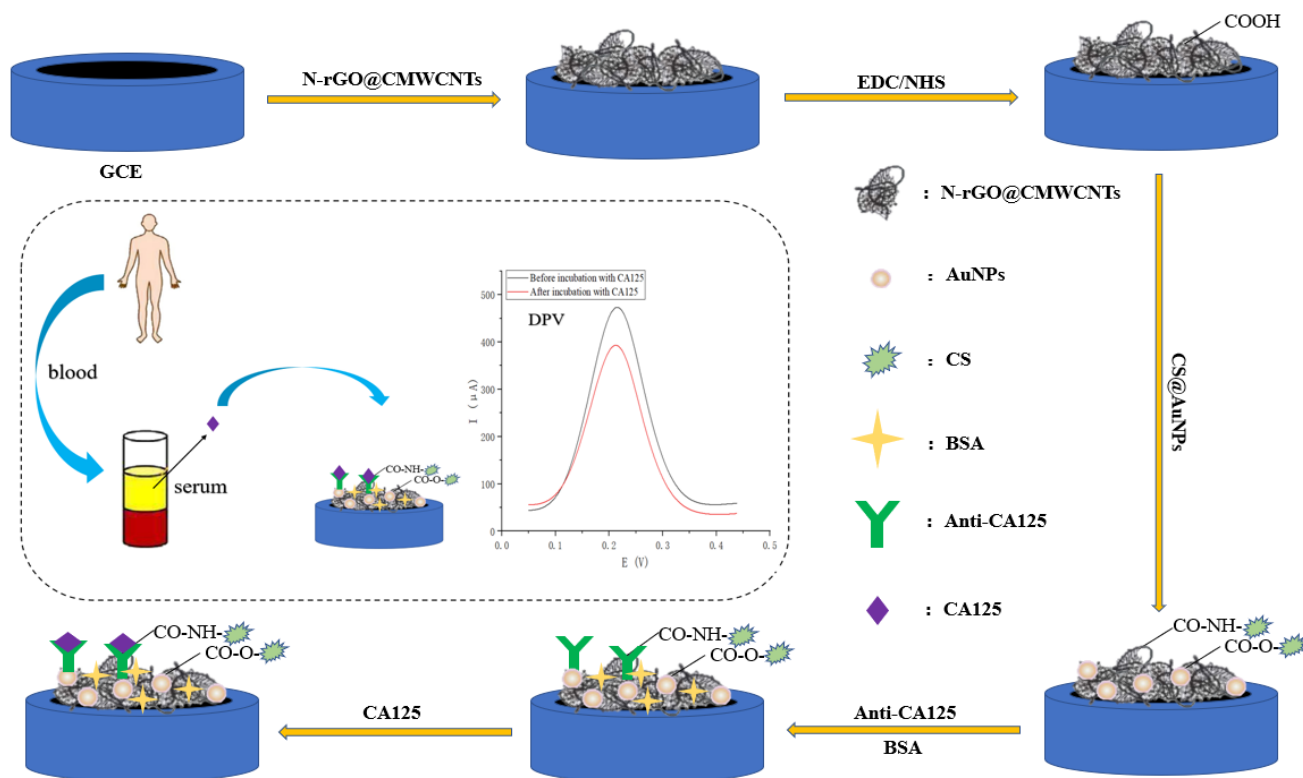


**Figure 1.** Construction of immunosensor.

### 3.2. Morphology Characterization

Figure 2 demonstrated the SEM images of N-rGO@CMWCNTs, CS@AuNPs and the modified electrode. As could be seen from Figure 2A, N-rGO had a sheet-like structure, while CMWCNTs presented a tubular structure with a diameter of about 15 nm. CMWCNTs prevented stacking between N-rGO sheets, and tubular CMWCNTs homogeneously compounded with sheet-like N-rGO, which could acquire a nanocomposite with ultra-high specific surface area and provide a lot of sites for subsequent materials to attach. As could be seen from Figure 2B, the synthesized AuNPs were uniformly dispersed in CS solution with a particle size of about 50 nm. Figure 2C,D were SEM images of the modified electrode, and it could be seen that N-rGO@CMWCNTs formed a complex three-dimensional structure on the surface of GCE, and a large number of AuNPs were attached to it. The above showed the successful synthesis of nano-modified materials, and the electrochemical performance of the modified electrode had great potential.

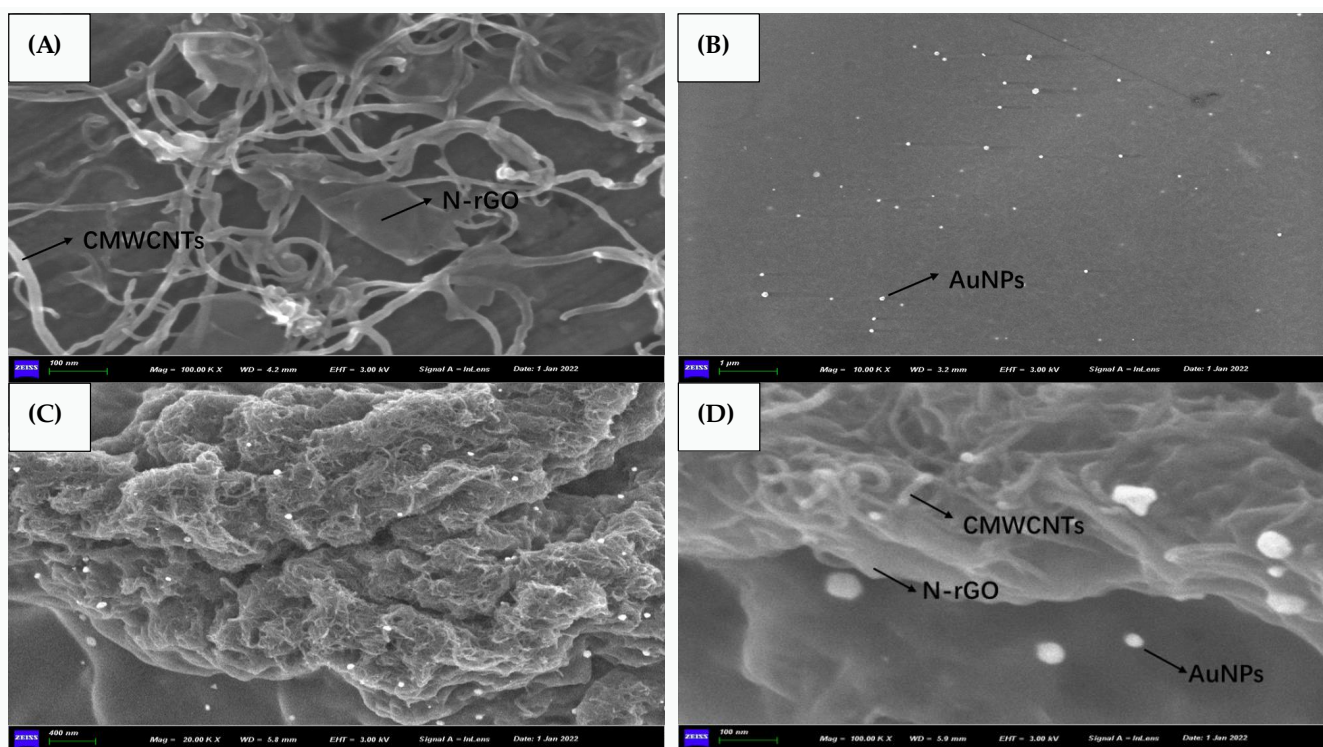


**Figure 2.** (A) SEM image of N-rGO@CMWCNTs; (B) SEM image of CS@AuNPs; and (C,D) SEM images of N-rGO@CMWCNTs/CS@AuNPs.

### 3.3. Electrochemical Characterization

To verify whether the immunosensing platform was successfully constructed, CV and DPV were used to characterize the modification process of GCE. The CV electrical signal of bare GCE was the smallest (curve a) shown in Figure 3. With the modification of N-rGO@CMWCNTs, the peak current increased significantly (curve b), indicating that the nanocomposite could enhance the electrical conductivity of the system. When CS@AuNPs were modified on the N-rGO@CMWCNTs/GCE, the peak current further increased (curve c); this was because AuNPs had extremely high electrical conductivity. The intensity of CV signal (curve c) from N-rGO@CMWCNTs/CS@AuNPs/GCE was higher than that of N-rGO/CS@AuNPs/GCE (curve m) and CMWCNTs/CS@AuNPs/GCE (curve n). However, when Anti-CA125 was incubated on N-rGO@CMWCNTs/CS@AuNPs/GCE, the peak current decreased significantly (curve d). As BSA and CA125 were incubated sequentially, since Anti-CA125, BSA and CA125 were all non-conductive biomacromolecules, they could bind, react, and accumulate on the electrode surface, which would hinder the electron transfer process and result in a further reduction of the peak current (curve e, curve f). Figure 4 showed the DPV signal intensities before and after incubation with CA125. Due to the specific immune reaction between Anti-CA125 and CA125, larger non-conductive immune complexes would be formed on the surface of GCE, which might reduce the electron transfer efficiency, leading to a decrease in DPV electric signal. Furthermore, as could be seen from Figure 4, compared with N-rGO/CS@AuNPs/GCE and CMWCNTs/CS@AuNPs/GCE, the N-rGO@CMWCNTs/CS@AuNPs/GCE could obtain a larger  $\Delta I$  ( $\Delta I = I_0 - I_p$ ,  $I_0$  was the peak current in the absence of CA125,  $I_p$  was the peak current in presence of  $0.1 \text{ ng mL}^{-1}$  CA125), presenting a better electrochemical performance.

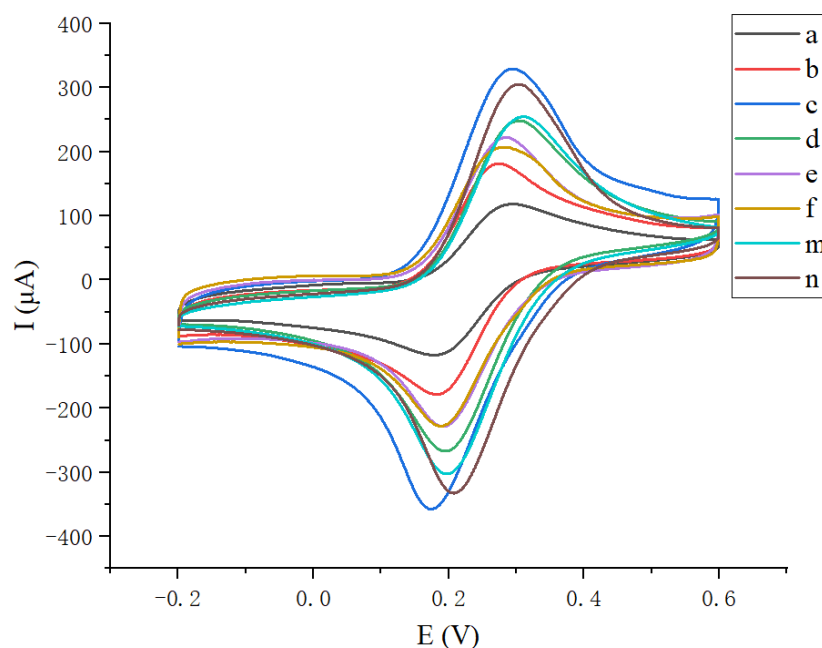


**Figure 3.** Cyclic voltammetry curves of bare GCE (curve **a**), N-rGO@CMWCNTs/GCE (curve **b**), N-rGO@CMWCNTs/CS@AuNPs/GCE (curve **c**), Anti-CA125/N-rGO@CMWCNTs/CS@AuNPs/GCE (curve **d**), BSA/Anti-CA125/N-rGO@CMWCNTs/CS@AuNPs/GCE (curve **e**), CA125/BSA/Anti-CA125/N-rGO@CMWCNTs/CS@AuNPs/GCE (curve **f**), N-rGO/CS@AuNPs/GCE (curve **m**), CMWCNTs/CS@AuNPs/GCE (curve **n**).

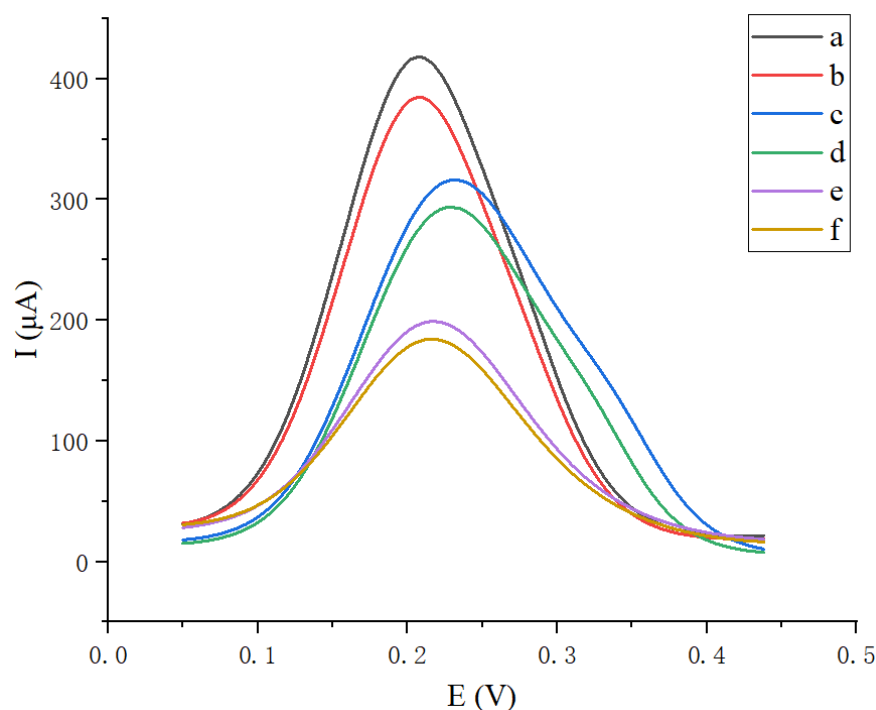


**Figure 4.** Differential pulse voltammetry curves of BSA/Anti-CA125/N-rGO@CMWCNTs/CS@AuNPs/GCE (curve **a**), CA125/BSA/Anti-CA125/N-rGO@CMWCNTs/CS@AuNPs/GCE (curve **b**), BSA/Anti-CA125/CMWCNTs/CS@AuNPs/GCE (curve **c**), CA125/BSA/Anti-CA125/CMWCNTs/CS@AuNPs/GCE (curve **d**), BSA/Anti-CA125/N-rGO/CS@AuNPs/GCE (curve **e**) and CA125/BSA/Anti-CA125/N-rGO/CS@AuNPs/GCE (curve **f**).

### 3.4. Optimization of Experimental Conditions

In order to obtain a highly sensitive and specific immunosensor for CA125 detection, experimental conditions were supposed to be optimized. The thickness of modified materials was an important factor affecting the experiment. When the amount of materials was too small, a complete and compact film could not be formed on the electrode surface, and the electrical signal amplification effect would correspondingly be weakened. When the amount of materials was too large, on one hand, their instability would be aggravated, and they could even fall off from the electrode surface; on the other hand, they would gather with each other, block the active sites on their surface, and reduce the efficiency of combination and reaction with other substances. Therefore, 2  $\mu\text{L}$ , 3  $\mu\text{L}$ , 4  $\mu\text{L}$ , 5  $\mu\text{L}$ , and 6  $\mu\text{L}$  of N-rGO@CMWCNTs were chosen to be added on the electrode surface, respectively; then, DPV was performed to observe the current signal  $\Delta I$ , and the max current signal was observed at 4  $\mu\text{L}$ . Similarly, the optimal amount of CS@AuNPs was determined to be 5  $\mu\text{L}$ . The incubation time and incubation concentration of Anti-CA125 were also key factors affecting the experimental results. If the incubation time was too short, Anti-CA125 would not fully bind to AuNPs; if the incubation time was too long, the biological activity of Anti-CA125 would be reduced. Meanwhile, as the incubation concentration gradually increased, the binding sites for Anti-CA125 were gradually saturated. Continuing to increase the concentration of Anti-CA125 would lead to the non-specific binding between them and reduce their binding efficiency with CA125. Therefore, 3 h, 6 h, 12 h, 16 h, and 24 h of incubation time and 10  $\mu\text{g mL}^{-1}$ , 25  $\mu\text{g mL}^{-1}$ , 50  $\mu\text{g mL}^{-1}$ , 75  $\mu\text{g mL}^{-1}$ , and 100  $\mu\text{g mL}^{-1}$  of incubation concentration were selected to be optimized. It turned out that the maximum current signals appeared at incubation time of 12 h and incubation concentration of 50  $\mu\text{g mL}^{-1}$ . These results were shown in Figure 5.

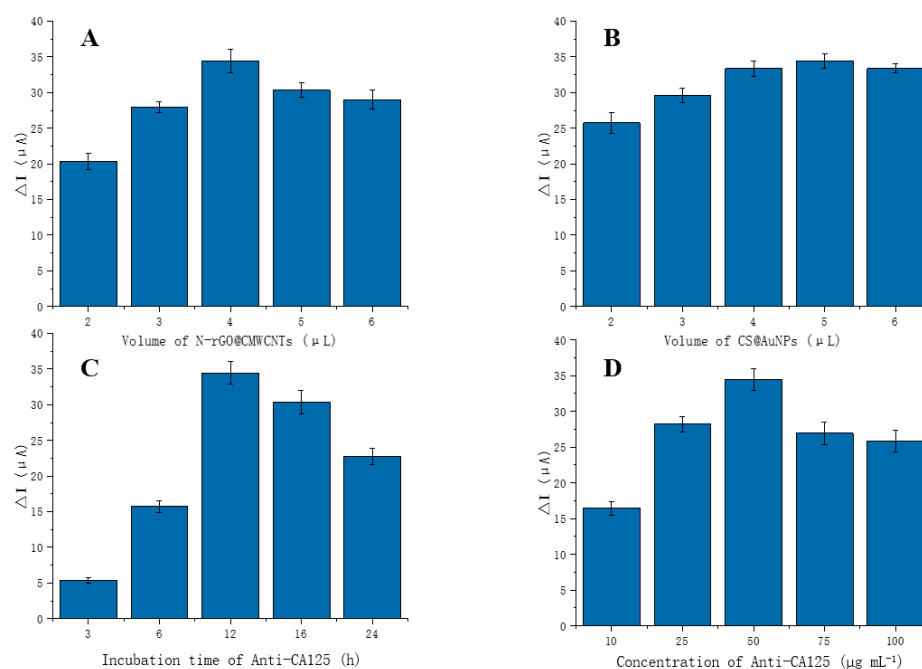


**Figure 5.** Optimization of experimental conditions (A) volume of N-rGO@CMWCNTs; (B) volume of CS@AuNPs; (C) incubation time of Anti-CA125; and (D) concentration of Anti-CA125.

### 3.5. Linear Range and Detection Limit

Under the optimal experimental conditions, the constructed immunosensor was tested by DPV to test its linear range and detection limit. As shown in Figure 6, when there was no CA125, the current signal was the largest; with the increase of CA125 concentration, the current signals gradually decreased. When the concentrations of CA125 were in the range of 0.1  $\mu\text{g mL}^{-1}$ –100  $\mu\text{g mL}^{-1}$ , there was a clear linear relationship between the change of

DPV current signal  $\Delta I$  ( $\Delta I = I_0 - I_p$ ,  $I_0$  was the peak current in the absence of CA125,  $I_p$  was the peak current in the presence of CA125) and the logarithm of CA125 with different concentrations ( $\lg C$   $\text{pg mL}^{-1}$ ). The linear equation was  $\Delta I = 8.0577 \lg C + 17.151$ , and the correlation coefficient ( $r$ ) was 0.997. The detection limit of this method was acquired by the ratio of three times standard deviation of the blank to the slope of standard curve ( $S/N = 3$ ), which was  $0.04 \text{ pg mL}^{-1}$ .

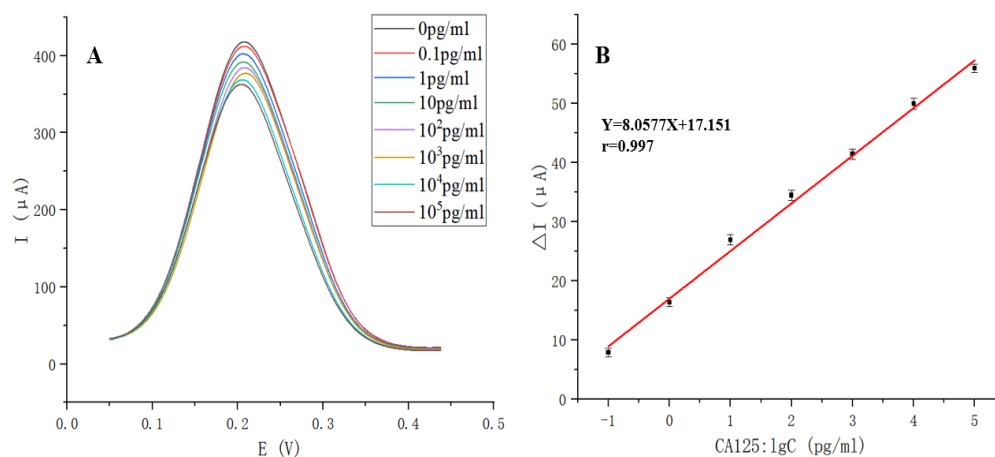


**Figure 6.** (A) DPV signals of CA125 with different concentrations; (B) the calibrated curve of the immunosensor toward different concentrations of CA125.

The analytical performance of the constructed immunosensing platform was compared with other reported electrochemical immunosensors for the CA125 assay, shown in Table 1. It could be seen that the immunosensing platform constructed in this research presented a lower detection limit and a wider linear range.

**Table 1.** Comparison of different electrochemical immunosensors for CA125 detection.

Type of Immunosensor	Method	Linear Range	LOD	Reference
PAMAM/AuNP-3DrGO-MWCNT nanocomposite modified GCE	SWV <sup>a</sup>	$0.5 \text{ mU mL}^{-1}$ – $75 \text{ U mL}^{-1}$	$6 \text{ μU mL}^{-1}$	[7]
ZnO nanorods-Au nanoparticles nanohybrids modified GCE	CV <sup>b</sup>	-	$2.5 \text{ μg mL}^{-1}$	[23]
AuNPs/GR modified SPCE	LSV <sup>c</sup>	$1 \text{ mU mL}^{-1}$ – $100 \text{ U mL}^{-1}$	$0.34 \text{ mU mL}^{-1}$	[24]
Cactus-like MnO <sub>2</sub> functionalized nanoporous gold modified GCE	SWV	$10 \text{ mU mL}^{-1}$ – $50 \text{ U mL}^{-1}$	$3.5 \text{ mU mL}^{-1}$	[25]
Metal sulfide quantum dot nanolabels and trifunctionalized magnetic beads modified GCE	SWASV <sup>d</sup>	$10 \text{ mU mL}^{-1}$ – $50 \text{ U mL}^{-1}$	$5 \text{ mU mL}^{-1}$	[26]
Thionine and gold nanoparticles supported on heteroatom-doped graphene nanocomposites modified GCE	DPV <sup>e</sup>	$3.2 \text{ mU mL}^{-1}$ – $10 \text{ U mL}^{-1}$	$0.28 \text{ U mL}^{-1}$	[27]
Benzothioephene derivative modified GCE	DPV	$1 \text{ ng mL}^{-1}$ – $100 \text{ ng mL}^{-1}$	$9.6 \text{ pg mL}^{-1}$	[28]
Gold-vertical graphene/TiO <sub>2</sub> nanotube modified GCE	DPV	$0.01 \text{ mU mL}^{-1}$ – $1 \text{ U mL}^{-1}$	$0.1 \text{ μU mL}^{-1}$	[29]
CMK-3(Au/Fc/MgAl-LDH)n multilayer nanocomposites modified GCE	DPV	$10 \text{ mU mL}^{-1}$ – $1000 \text{ U mL}^{-1}$	$4 \text{ mU mL}^{-1}$	[30]
Nickel hexacyanoferrate nanocubes/polydopamine functionalized graphene modified GCE	DPV	$0.1 \text{ pg mL}^{-1}$ – $1 \text{ μg mL}^{-1}$	$0.076 \text{ pg mL}^{-1}$	[31]
FA, H-PANI and CS-HCl modified GCE	SWV	$1 \text{ pg mL}^{-1}$ – $25 \text{ ng mL}^{-1}$	$0.25 \text{ pg mL}^{-1}$	[32]
Electrochemical aptasensing platform based on combination of target-triggered SDA and aptamer recognition	SWV	$50 \text{ pg mL}^{-1}$ – $50 \text{ ng mL}^{-1}$	$5 \text{ pg mL}^{-1}$	[33]
Hybridization chain reaction and biotin-streptavidin signal amplification strategy	DPV	$0.2 \text{ pg mL}^{-1}$ – $1 \text{ ng mL}^{-1}$	$0.08 \text{ pg mL}^{-1}$	[34]
N-rGO@CMWCNTs/CS@AuNPs modified GCE	DPV	$0.1 \text{ pg mL}^{-1}$ – $100 \text{ ng mL}^{-1}$	$0.04 \text{ pg mL}^{-1}$	This work

<sup>a</sup> Square wave voltammetry; <sup>b</sup> Cyclic voltammetry; <sup>c</sup> Linear sweep voltammetry; <sup>d</sup> Square wave anodic stripping voltammetry; <sup>e</sup> Differential pulse voltammetry.



### 3.6. Reproducibility, Stability, and Selectivity

To test the reproducibility of the constructed immunosensor, three glassy carbon electrodes prepared by the same method were used to measure  $0.1 \text{ ng mL}^{-1}$  CA125. The relative standard deviation (RSD) of the assay results as shown in Figure 7A was 4.23%, which indicated that the proposed immunosensor had a good reproducibility.

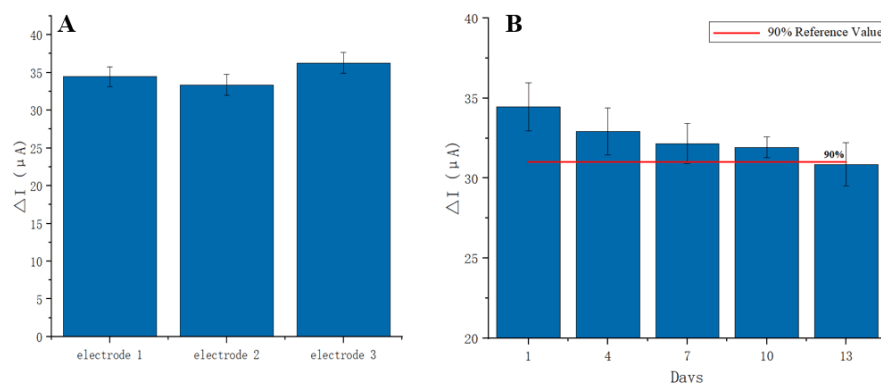


**Figure 7.** (A) Reproducibility and (B) stability of the immunosensor.

For the stability test, a modified electrode was used to measure  $0.1 \text{ ng mL}^{-1}$  CA125. The measurement was taken every three days, followed by repeating for 13 days. After each measurement, the modified electrode was washed with PBS and stored at  $4 \text{ }^\circ\text{C}$ . The results were shown in Figure 7B, and it could be seen that the immunosensor maintained 90% of its initial signal for 10 days, which showed that the immunosensor presented acceptable stability.

When detecting CA125 in serum, other common substances in serum might interfere with the experimental results, so the selectivity of the immunosensor was also investigated. In addition,  $800 \text{ } \mu\text{g mL}^{-1}$  glucose (Glu),  $10 \text{ } \mu\text{g mL}^{-1}$  ascorbic acid (AA),  $50 \text{ } \mu\text{g mL}^{-1}$  uric acid (UA) and  $10 \text{ ng mL}^{-1}$  CYFRA21-1 were chosen to investigate their interference, and these selected concentrations were similar to or higher than that in patients with lung cancer. The results were shown in Figure 8, from which we could find that the DPV signals of these interfering substances were much lower than that of  $0.1 \text{ ng mL}^{-1}$  CA125, and it was attributed to the specific recognition between Anti-CA125 and CA125. The above results indicated that the constructed immunosensor had a good selectivity to target analyte CA125.

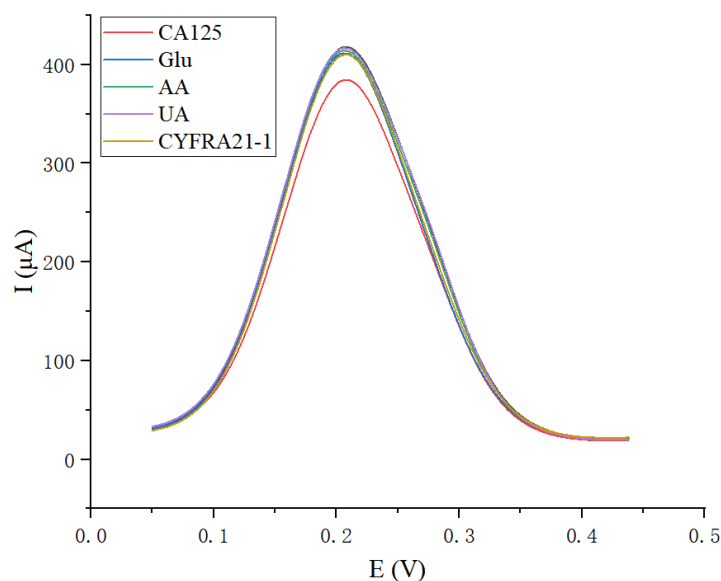


**Figure 8.** Differential pulse voltammetry curves of various interfering substances and CA125.

### 3.7. Analysis of Real Serum Samples

To evaluate the feasibility of the constructed immunosensor in detection of real serum samples, a spike recovery experiment was carried out. In addition, 1 ng mL<sup>-1</sup>, 10 ng mL<sup>-1</sup>, and 100 ng mL<sup>-1</sup> CA125 standard solutions were added to healthy human serum separately, followed by diluting 100-fold with PBS; the same measurement method as above was then performed. The results were shown in Table 2, from which it could be found that the recoveries were in the range of 94.5–107.7% with the corresponding RSD in the range of 3.88–7.07%, demonstrating that this method was reliable.

**Table 2.** Recovery results of the constructed immunosensor.

No	Added (pg mL <sup>-1</sup> )	Found (pg mL <sup>-1</sup> )	Recovery	RSD (N = 3)
1	10	10.39	103.9%	7.07%
2	100	107.72	107.7%	4.17%
3	1000	945.16	94.5%	3.88%

Moreover, serum samples from 10 patients with lung cancer were diluted 100-fold with PBS, and then detected using this immunosensor. The results were in the range of 13.90 pg mL<sup>-1</sup>–25.88 ng mL<sup>-1</sup> with the corresponding RSD in the range of 4.65–7.22%. These acceptable results indicated that the constructed immunosensor had potential for the detection of serum samples in clinical.

## 4. Conclusions

In this research, a novel electrochemical immunosensor was fabricated by using N-rGO@CMWCNTs/CS@AuNPs modified GCE, which could achieve ultrasensitive detection of CA125. The N-rGO@CMWCNTs with high specific surface area and great conductivity were used as a matrix, providing a large number of binding sites for CS@AuNPs. Meanwhile, the chemical groups from CS and CMWCNTs could react with each other, promoting the close binding between N-rGO@CMWCNTs and CS@AuNPs, which achieved co-amplification of electric signals and greatly improved the sensitivity of the electrochemical immunosensor. Furthermore, Anti-CA125 reacted with AuNPs via sulfhydryl groups (-SH) to form Au-S bonds, which was further able to form an immune complex with CA125. The constructed immunosensor presented excellent performance with the linear range of 0.1 pg mL<sup>-1</sup>–100 ng mL<sup>-1</sup> and an LOD of 0.04 pg mL<sup>-1</sup>, and it also exhibited satisfactory reproducibility, acceptable stability, and high selectivity. In addition, the novel immunosensor exhibited excellent ability for detecting CA125 in serum from lung cancer patients, and the newly established method had great potential for early diagnosis of lung cancer.

**Author Contributions:** Conceptualization, Y.G.; methodology, Y.G.; experimental operation, G.G. and Y.J.; software, G.G. and J.Q.; data curation, Y.J. and J.Q.; writing—original draft, Y.G. and G.G.; writing—review and editing, Y.M. and J.H.; resources, Y.M.; project administration, J.H.; funding acquisition, Y.M. and J.H. All authors have read and agreed to the published version of the manuscript.

**Funding:** This work was supported by the National Natural Science Foundation of China (No. 81973097).

**Institutional Review Board Statement:** The study was conducted in accordance with the guidelines of the Declaration of Helsinki, and was approved by the Ethical Committee of Wuhan University of Science and Technology.

**Informed Consent Statement:** Informed consent was obtained from all subjects involved in the study.

**Data Availability Statement:** Not applicable.

**Acknowledgments:** We highly appreciate Hongzhi Pan from Shanghai University of Medicine and Health Sciences for the technical support and funding acquisition. The characterization of this work has also been supported by the SouSePad Test Scientific Research Service.

**Conflicts of Interest:** The authors declare no conflict of interest.

## References

1. Joseph, E.T.; Agnihotram, V.R.; Eduardo, L.F. Lung cancer screening: Review and performance comparison under different risk scenarios. *Lung* **2014**, *192*, 55–63.
2. Rastogi, A.; Yadav, K.; Mishra, A.; Singh, M.S.; Chaudhary, S.; Manohar, R.; Parmar, A.S. Early diagnosis of lung cancer using magnetic nanoparticles-integrated systems. *Nanotechnol. Rev.* **2022**, *11*, 544–574. [[CrossRef](#)]
3. Wulfkuhle, J.D.; Liotta, L.A.; Petricoin, E.F. Proteomic applications for the early detection of cancer. *Nat. Rev. Cancer.* **2003**, *3*, 267–275. [[CrossRef](#)] [[PubMed](#)]
4. Wang, Y.F.; Wu, R.; Kathleen, R.C.; Dafydd, G.T.; Gabrielle, G.; Rebecca, J.L.; Thomas, J.G.; Kerby, A.S.; David, E.M.; David, M.L. Differential protein mapping of ovarian serous adenocarcinomas: Identification of potential markers for distinct tumor stage. *J. Proteome Res.* **2009**, *8*, 1452–1463. [[CrossRef](#)] [[PubMed](#)]
5. Pujol, J.L.; Boher, J.M.; Grenier, J.; Quantin, X. Cyfra 21-1, neuron specific enolase and prognosis of non-small cell lung cancer: Prospective study in 621 patients. *Lung Cancer* **2001**, *31*, 221–231. [[CrossRef](#)]
6. Amy, E.L.; Mary, E.F.; Geri, H.; Paige, H.; Amanda, O.; Amin, A. Understanding the value of tumor markers in pediatric ovarian neoplasms. *J. Pediatr. Surg.* **2019**, *55*, 122–125.
7. Parvin, S.P.; Marziyeh, F.; Hossein, G.; Reza, S.; Yadollah, O. A novel electrochemical immunosensor for ultrasensitive detection of CA125 in ovarian cancer. *Biosens. Bioelectron.* **2020**, *153*, 112029.
8. He, Z.; Ning, G.; Jin, W. Determination of tumor marker CA125 by capillary electrophoretic enzyme immunoassay with electrochemical detection. *Anal. Chim. Acta* **2003**, *497*, 75–81. [[CrossRef](#)]
9. Li, Y.; Wang, Z.C.; Luo, L.; Mu, C.Y.; Xu, J.; Feng, Q.; Li, S.B.; Gu, B.; Ma, P.; Lan, T. The clinical value of the combined detection of sEGFR, CA125 and HE4 for epithelial ovarian cancer diagnosis. *Eur. Rev. Med. Pharmacol. Sci.* **2020**, *24*, 604–610.
10. Ge, L.; Wang, P.P.; Ge, S.G.; Li, N.Q.; Yu, J.H.; Yan, M.; Huang, J.D. Photoelectrochemical lab-on-paper device based on an integrated paper supercapacitor and internal light source. *Anal. Chem.* **2013**, *85*, 3961–3970. [[CrossRef](#)]
11. Samaneh, R.; Abolfazl, M.K.; Shahla, C.; Ali-Akbar, D.; Leila, A.; Mahin, A.P.; Sepideh, K.; Ibrahim, A. The diagnostic accuracy of combined enolase/Cr, CA125, and CA19-9 in the detection of endometriosis. *Biomed. Res. Int.* **2020**, *2020*, 5208279.
12. Jie, W.; Fu, Z.; Feng, Y.; Ju, H. Biomedical and clinical applications of immunoassays and immunosensors for tumor markers. *Trends Anal. Chem.* **2007**, *26*, 679–688.
13. Chandrakala, G.; Kumarasamy, J.; Archana, D.; Savita, K.; Meera, V.; Sharmila, B.; Rajan, M.G.R. Comparison of serum thyroglobulin levels in differentiated thyroid cancer patients using in-house developed radioimmunoassay and immunoradiometric procedures. *Indian J. Clin. Biochem.* **2019**, *34*, 465–471.
14. Fabiana, S.F.; Lúcio, A. Electrochemical immunosensors: A powerful tool for analytical applications. *Biosens. Bioelectron.* **2018**, *102*, 470–478.
15. Lai, Y.X.; Wang, L.J.; Liu, Y.; Yang, G.J.; Tang, C.L.; Deng, Y.; Li, S. Immunosensors based on nanomaterials for detection of tumor markers. *J. Biomed. Nanotechnol.* **2018**, *14*, 44–65. [[CrossRef](#)] [[PubMed](#)]
16. Niu, Y.L.; Yang, T.; Ma, S.S.; Peng, F.; Yi, M.H.; Wan, M.M.; Mao, C.; Shen, J. Label-free immunosensor based on hyperbranched polyester for specific detection of  $\alpha$ -fetoprotein. *Biosens. Bioelectron.* **2017**, *92*, 1–7. [[CrossRef](#)]
17. Kesarwani, S.; Verma, R.K. A critical review on synthesis, characterization and multifunctional applications of reduced graphene oxide (rGO)/composites. *Nano* **2021**, *16*, 2130008. [[CrossRef](#)]
18. Tian, Y.; Wang, F.; Liu, Y.; Pang, F.; Zhang, X. Green synthesis of silver nanoparticles on nitrogen-doped graphene for hydrogen peroxide detection. *Electrochim. Acta* **2014**, *146*, 646–653. [[CrossRef](#)]
19. Huang, Z.Y.; Chen, H.; Ye, H.R.; Chen, Z.X.; Nicole, J.R.; Guo, Z.Z. An ultrasensitive aptamer-antibody sandwich cortisol sensor for the noninvasive monitoring of stress state. *Biosens. Bioelectron.* **2021**, *190*, 113451. [[CrossRef](#)]
20. Alle, M.; Gangapuram, B.R.; Maragoni, V.; Guttana, V.; Dudde, A.K.; Sumathi, N.; Ming-Yeh, Y.; Anren, H.; Surya, S.S. Efficient pH dependent drug delivery to target cancer cells by gold nanoparticles capped with carboxymethyl chitosan. *Int. J. Mol. Sci.* **2014**, *15*, 8216–8234.
21. Singh, A.; Sinsinbar, G.; Choudhary, M.; Kumar, V.; Pasricha, R.; Verma, H.N.; Surinder, P.S.; Arora, K. Graphene oxide-chitosan nanocomposite based electrochemical DNA biosensor for detection of typhoid. *Sens. Actuators B Chem.* **2013**, *185*, 675–684. [[CrossRef](#)]
22. Parvin, S.P.; Hossein, G.; Reza, S.; Yadollah, O. Electrochemical immunosensor based on chitosan-gold nanoparticle/carbon nanotube as a platform and lactate oxidase as a label for detection of CA125 oncomarker. *Biosens. Bioelectron.* **2018**, *122*, 68–74.
23. Gisane, G.; Costa, J.P.C.; Costa, P.I.; Zaghete, M.A.; Mazon, T. Electrochemical immunosensor based on ZnO nanorods-Au nanoparticles nanohybrids for ovarian cancer antigen CA-125 detection. *Mater. Sci. Eng. C* **2017**, *76*, 1240–1247.
24. Ge, S.G.; Yu, F.; Ge, L.; Yan, M.; Yu, J.H.; Chen, D.R. Disposable electrochemical immunosensor for simultaneous assay of a panel of breast cancer tumor markers. *Analyst* **2012**, *137*, 4727. [[CrossRef](#)]
25. Zhang, Y.; Li, L.; Lu, J.J.; Ge, L.; Ge, S.G.; Yan, M.; Song, X.R.; Yu, J.H. Triple catalysis amplification strategy for simultaneous multiplexed electrochemical immunoassays based on cactus-like MnO<sub>2</sub> functionalized nanoporous gold. *Sens. Actuators B Chem.* **2013**, *186*, 545–549. [[CrossRef](#)]
26. Tang, D.P.; Hou, L.; Reinhard, N.; Xu, M.D.; Gao, Z.Q.; Dietmar, K. Multiplexed electrochemical immunoassay of biomarkers using metal sulfide quantum dot nanolabels and trifunctionalized magnetic beads. *Biosens. Bioelectron.* **2013**, *46*, 37–43. [[CrossRef](#)]

27. Maalavika, S.L.; Wang, F.M.; Ilangovan, R. Electrochemical detection of CA125 using thionine and gold nanoparticles supported on heteroatom-doped graphene nanocomposites. *Appl. Nanosci.* **2021**, *11*, 2167–2180.
28. Omer, F.E.; Hilal, K.; Omrueye, O.; Sebahattin, C.; Arif, K. A novel electrochemical sensor for monitoring ovarian cancer tumor protein CA125 on benzothiophene derivative based electrodes. *J. Electroanal. Chem.* **2022**, *904*, 115854.
29. Chen, Z.H.; Li, B.B.; Liu, J.B.; Li, H.J.; Li, C.P.; Xuan, X.W.; Li, M.J. A label-free electrochemical immunosensor based on a gold–vertical graphene/TiO<sub>2</sub> nanotube electrode for CA125 detection in oxidation/reduction dual channels. *Microchim. Acta* **2022**, *189*, 257. [[CrossRef](#)]
30. Wu, M.D.; Liu, S.M.; Qi, F.F.; Qiu, R.; Feng, J.; Ren, X.S.; Rong, S.Z.; Ma, H.K.; Chang, D.; Pan, H.Z. A label-free electrochemical immunosensor for CA125 detection based on CMK-3(Au/Fc@MgAl-LDH)<sub>n</sub> multilayer nanocomposites modification. *Talanta* **2022**, *241*, 123254. [[CrossRef](#)]
31. Zhang, F.L.; Fan, L.F.; Liu, Z.G.; Han, Y.J.; Guo, Y.J. A label-free electrochemical aptasensor for the detection of cancer antigen 125 based on nickel hexacyanoferrate nanocubes/polydopamine functionalized graphene. *J. Electroanal. Chem.* **2022**, *918*, 116424. [[CrossRef](#)]
32. Ren, X.; Wang, H.; Wu, D.; Fan, D.W.; Zhang, Y.; Du, B.; Wei, Q. Ultrasensitive immunoassay for CA125 detection using acid site compound as signal and enhancer. *Talanta* **2015**, *144*, 535–541. [[CrossRef](#)] [[PubMed](#)]
33. Chen, J.S.; Hu, W.B.; Wei, J.; Yu, F.; Wu, L.; Wang, C.M.; Wang, W.; Zuo, S.Y.; Shang, B.; Chen, Q.H. An electrochemical aptasensing platform for carbohydrate antigen 125 based on the use of flower-like gold nanostructures and target-triggered strand displacement amplification. *Microchim. Acta* **2019**, *388*, 186. [[CrossRef](#)] [[PubMed](#)]
34. Zhu, Q.; Chai, Y.Q.; Zhuo, Y.; Yuan, R. Ultrasensitive simultaneous detection of four biomarkers based on hybridization chain reaction and biotin-streptavidin signal amplification strategy. *Biosens. Bioelectron.* **2015**, *68*, 42–48. [[CrossRef](#)] [[PubMed](#)]